JPE 18-2-3

https://doi.org/10.6113/JPE.2018.18.2.343
ISSN(Print): 1598-2092 / ISSN(Online): 2093-4718

A Wide Voltage-Gain Range Asymmetric H-Bridge Bidirectional DC-DC Converter with a Common Ground for Energy Storage Systems

Yun Zhang[†], Yongping Gao[*], Jing Li[**], and Mark Sumner[***]

[†,*]School of Electrical and Information Engineering, Tianjin University, Tianjin, China
[**]Department of Electrical and Electronic Engineering, University of Nottingham Ningbo China, Ningbo, China
[***]Department of Electrical and Electronic Engineering, University of Nottingham, Nottingham, ENG, UK

Abstract

A wide-voltage-conversion range bidirectional DC-DC converter is proposed in this paper. The topology is comprised of one typical *LC* energy storage component and a special common grounded asymmetric H-bridge with four active power switches/anti-parallel diodes. The narrow output PWM voltage is generated from the voltage difference between two normal (wider) output PWM voltages from the asymmetric H-bridge with duty cycles close to 0.5. The equivalent switching frequency of the output PWM voltage is double the actual switching frequency, and a wide step-down/step-up ratio range is achieved. A 300W prototype has been constructed to validate the feasibility and effectiveness of the proposed bidirectional converter between the variable low voltage side (24V~48V) and the constant high voltage side (200V). The slave active power switches allow ZVS turn-on and turn-off without requiring any extra hardware. The maximum conversion efficiency is 94.7% in the step-down mode and 93.5% in the step-up mode. Therefore, the proposed bidirectional topology with a common ground is suitable for energy storage systems such as renewable power generation systems and electric vehicles with a hybrid energy source.

Key words: Asymmetric H-bridge, Bidirectional DC-DC converter, Common ground, Energy storage systems, Wide voltage-gain range

I. INTRODUCTION

The twin challenges associated with fossil fuels, the diminishing resources available worldwide and the increasingly serious environment pollution associated with these fuels, mean that renewable power generation and the electrification of transportation can be seen as efficient ways to address these challenges [1]-[4]. In renewable power generation systems, high energy/power density storage devices, such as batteries and super-capacitor banks, are very important for the smoothing of energy fluctuations through peak load shifting [5], [6]. In hybrid energy source electric vehicles, high power density super-capacitor banks are used to provide the high instantaneous power required for acceleration and braking processes, and high energy density battery banks deal with the stable or low frequency components of energy to and from the DC-link side [7], [8] or "steady state" power. As a result, the battery bank can be operated in a healthy manner to maintain a long-life. In addition, an excellent dynamic response and energy conversion efficiency can also be achieved. However, bidirectional DC-DC converters are required to buffer the energy between the high voltage DC-link side (200V to 400V) and the low voltage energy storage side (24V to 48V) in renewable power generation systems and hybrid energy source electric vehicles. Therefore, the voltage-conversion range of the selected bidirectional DC-DC converter is approximately between 5 and 10.

In applications that require galvanic isolation, the dual active full-bridge DC-DC converter can obtain the required high voltage-gain by using an appropriate turns ratio between the primary and secondary sides of the high frequency transformer [9]. However, the large turns ratio of this transformer at high

Manuscript received May 29, 2017; accepted Oct. 15, 2017
Recommended for publication by Associate Editor Yan Xing.
[†]Corresponding Author: zhangy@tju.edu.cn
Tel: +86-0130-3221-0767, Tianjin University
[*]School of Electrical and Information Eng., Tianjin University, China
[**]Dept. Electrical Electron. Eng., Univ. of Nottingham Ningbo China, China
[***]Dept. Electrical Electron. Eng., Univ. of Nottingham, ENG, UK

power levels creates the following problems [10]: reduced coupling, core losses from non-sinusoidal (i.e. high frequency AC square wave) excitation and dielectric losses in the insulation. In addition, the distributed capacitance of the winding turns reduces the efficiency. When the input and output voltages cannot match the turns ratio of the transformer, the switching loss increases dramatically [11]. In applications that do not require isolation, DC-DC converters with a coupled-inductor can have a higher voltage-gain, and reduce the reverse recovery losses of the diodes [12], [13]. However, it is difficult to design coupled-inductors (and high frequency transformers) at these high power levels. Although the converter in [14] achieved ZVS for all of the active switches, it still needs a coupled-inductor, and fails to achieve a bidirectional power flow. In addition, the input current ripple is considerable due to the operation of the coupled-inductor, which may result in a shorter cycle life of the energy storage devices, as well as a reduction in efficiency. For the conventional bidirectional DC-DC converter, there are extreme voltage stresses across the active power switches and diodes when extreme duty cycles are used [15]. This results in serious EMI issues and reverse recovery losses, as well as a lower conversion efficiency. The converters in [16] and [17] can achieve a higher voltage-gain. However, the maximum voltage stress of the power switch in [16] is higher than that of the high voltage side, and the converter in [17] needs an auxiliary circuit that includes a capacitor and an inductor to achieve high efficient power conversion. The Cuk and Sepic/Zeta conversion efficiencies are lower, due to the cascaded configurations of the two power stages [18], [19]. In [20], a high efficiency and high voltage-gain DC-DC converter with soft-switching was proposed. However, it has a complex coupled-inductor and associated circuits. The soft-switching DC-DC converter proposed [21] can operate over a wide load range. However, its conversion ratio is not high enough for the proposed applications. In [22], a converter is proposed that combines soft-switching and hard-switching techniques and can improve the conversion efficiency. However, it needs extra semiconductors and a coupled-inductor. An interleaved high conversion-ratio bidirectional DC-DC converter was proposed for distributed energy-storage systems in [23]. However, its high conversion-ratio was obtained by adding switched-capacitors and coupled-inductors in series. It also requires more active power switches, capacitors and coupled-inductors, and is not cost effective. In order to reduce the input current ripple, interleaved switched-capacitor converters have been proposed in [24], [25]. However, the converter in [24] fails to achieve soft-switching, and the converter in [25] suffers from a huge current ripple in the low-voltage side. Through a switched-capacitor cell, the converter in [26] achieved a high voltage conversion ratio. Unfortunately, a potential difference between the output and the input side grounds exists in the high frequency PWM voltage, which makes it unsuitable for energy storage systems.

In addition to the DC-DC converters with transformers, the coupled-inductors and the switched-capacitors mentioned above, a group of DC-DC converters exists which uses the Z-source structure, which can improve the step-up/step-down ratio [27]. High voltage-gain DC-DC converters with a Z-source structure do not have a common ground between the input side and the output side, because the boost inductor is directly replaced by the Z-source. However, common grounded DC-DC converters are required for renewable power generation systems and hybrid energy source electric vehicles, due to safety concerns (especially during maintenance). In addition, they can reduce EMI issues. Therefore, a common grounded Z-source DC-DC converter with a high voltage-gain was proposed in [28] based on the above mentioned Z-source DC-DC converter. However, this common grounded Boost DC-DC converter has not been applied to energy storage systems or hybrid energy source electric vehicles. Moreover, its input current is discontinuous due to the input diode for the Z-source.

In this paper, a bidirectional DC-DC converter for the energy storage systems in renewable energy and electric vehicle systems is proposed. It is comprised of one LC energy storage component and four active power switches with the anti-parallel diodes. This avoids the need for a transformer, a coupled-inductor, and a switched-capacitor or a Z-source impedance net. A high step-up/step-down ratio can be obtained by using non-extreme duty cycles for the four active power switches. In addition, the low and high voltage sides have a common ground, and the input/output currents on the low voltage side (i.e. battery or super-capacitor banks) are continuous. This paper is structured as follows. In Section II, the proposed topology is demonstrated. The operating principle is explained in Section III, and experimental results and analysis are presented in Section IV. Finally, some conclustions are given in Section V.

II. TOPOLOGY

The evolution process of the proposed topology in this paper is presented in Fig. 1. As with the conventional common grounded bidirectional DC-DC converter (i.e. the buck/boost DC-DC converter), it is comprised of one bidirectional power cell (i.e. a half bridge) as shown in Fig. 1(a). The bidirectional H-bridge DC-DC converter can be synthesized by connecting two bidirectional power cells in parallel [29]. The output PWM voltage U_{ab} can be given as:

$$U_{ab} = U_{ag} - U_{bg} \tag{1}$$

where the points "a" and "b" are the output ports of the left and right half bridges, respectively, and point "g" is the ground of the high voltage side U_h. In addition, U_{ag} is the voltage stress of the active power switch Q_2, and U_{bg} is the voltage stress of the active power switch Q_4. In terms of (1), the non-extreme output PWM voltages U_{ag} and U_{bg} can be obtained when the duty

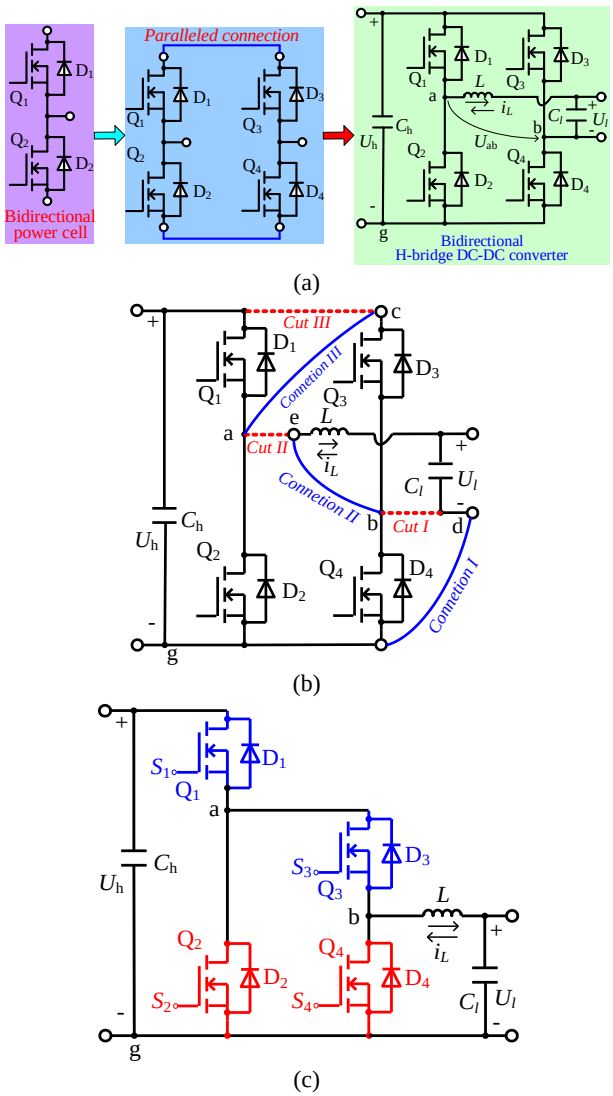

Fig. 1. The evolution process of the proposed topology. (a) Bidirectional H-bridge DC-DC converter without a common ground [29]. (b) Evolution process of the proposed topology. (c) Proposed bidirectional DC-DC converter with a common grounded asymmetric H-bridge.

cycles of the active power switches are around 0.5. The PWM voltage difference U_{ab} between U_{ag} and U_{bg} becomes extremely small, i.e. a high step-up or step-down ratio is achieved. However, there is a problem in the topology of the bidirectional H-bridge DC-DC converter shown in Fig. 1(a). The high and the low voltage sides do not have a common ground. Therefore, EMI issues can occur and maintenance can be unsafe in real applications. Furthermore, the bidirectional H-bridge DC-DC converter without a common ground in Fig. 1(a) cannot be extended to the interleaved bidirectional DC-DC converters for higher power levels.

Therefore, a common grounded topology is derived as shown in Fig. 1(b). First, the ground "d" of the low voltage side U_l should be disconnected from point "b" (i.e. *Cut I*), and point "d" connects the ground "g" of the high voltage side U_h directly (*Connection I*). Then, the left point "e" of the inductor L should be also disconnected from point "a" (i.e. *Cut II*), and point "e" connects the output port "b" of the right half bridge directly (*Connection II*). Finally, in order to obtain an extremely narrow PWM voltage U_{bg} between the points "b" and "g", U_{bg} can be achieved by (1) as:

$$U_{bg} = U_{ag} - U_{ab} \tag{2}$$

Therefore, point "c" should still be disconnected from the positive port of the high voltage side (i.e. *Cut III*), and point "c" connects the output port "a" of the left half bridge directly (*Connection III*). As a result, a bidirectional DC-DC converter with a common grounded asymmetric H-bridge is proposed as shown in Fig. 1(c). D_1~D_4 are the corresponding anti-parallel diodes of the MOSFETs Q_1~Q_4, and S_1~S_4 are the gate signals for Q_1~Q_4. L is the energy storage inductor, and C_h and C_l are the filter capacitors of U_h and U_l, respectively.

III. Operating Principle

A. Bidirectional Operation States

In the proposed converter, shown in Fig. 1(c), the switching state "S_x=1" stands for the active power switch Q_X "*ON*", where x=1, 2, 3 and 4. Otherwise, "S_x=0" represents Q_X "*OFF*". It is worth noting that Q_1 and Q_3 act as master active power switches when the power flow is from U_h to U_l, i.e. Q_2 and Q_4 are slave active power switches (S_2S_4=00) in the step-down mode. In this mode, the states of the converter's components are shown in Table I. Therefore, Q_1 and Q_3 are *ON* and Q_2, Q_4 and D_1~D_4 are all *OFF* when $S_1S_2S_3S_4$=1010. The inductor current i_L flows in Q_1 and Q_3, L is charged by U_h, and the output PWM voltage is U_{bg}=U_h. When $S_1S_2S_3S_4$=1000, Q_1 and D_4 are *ON*, and Q_2~Q_4 and D_1~D_3 are all *OFF*. However, i_L flows in D_4 rather than Q_1, due to the freewheeling requirement of the inductor. Therefore, L is discharged into the load, and U_{bg}=0. When $S_1S_2S_3S_4$=0010, Q_3, D_2 and D_4 are *ON*, and Q_1, Q_2, Q_4, D_1 and D_3 are *OFF*. One part of i_L flows in D_2 and Q_3 in series, and the other part of i_L flows in D_4. As a result, L continues to discharge into the load and U_{bg}=0.

When the power flow is from U_l to U_h, Q_1 and Q_3 are slave active power switches (S_1S_3=00) in the step-up mode, and Q_2 and Q_4 act as master active power switches. In this step-up mode, the states of the converter's components are shown in Table II. When $S_1S_2S_3S_4$=0000, D_1 and D_3 are *ON*, Q_1~Q_4, D_2 and D_4 are *OFF*. i_L flows in D_3 and D_1 in series, L discharges into the load, and U_{bg}=U_h. When $S_1S_2S_3S_4$=0100, Q_2 and D_3 are *ON*, Q_1, Q_3, Q_4, D_1, D_2 and D_4 are *OFF*. i_L flows in D_3 and Q_2 in series, L is charged by U_l, and U_{bg}=0. When $S_1S_2S_3S_4$=0001, only Q_4 is *ON*, L is charged by U_l through Q_4, and U_{bg}=0.

B. Operating for a Wide-Voltage-Conversion Range

The PWM modulation strategy for the proposed converter in the step-down mode is shown in Fig. 2. The gate signals S_1 and S_3 for the master active power switches Q_1 and Q_3 are defined as:

TABLE I
COMPONENT STATES WHEN THE POWER FLOW IS FROM UH TO UL (STEP-DOWN)

Master power switches	S_1S_2 S_3S_4	*L*	D_1	D_2	D_3	D_4	U_{bg}
Q_1 and Q_3	**1**0**1**0	*ch.*	*OFF*	*OFF*	*OFF*	*OFF*	U_h
	10**0**0	*dis.*	*OFF*	*OFF*	*OFF*	*ON*	0
	00**1**0	*dis.*	*OFF*	*ON*	*OFF*	*ON*	0

**Annotate*: "*ch.*" and "*dis.*" mean "charged" and "discharged" energy, respectively.

TABLE II
COMPONENT STATES WHEN THE POWER FLOW IS FROM U_L TO U_H (STEP-UP)

Master power switches	S_1S_2 S_3S_4	*L*	D_1	D_2	D_3	D_4	U_{bg}
Q_2 and Q_4	0**0**0**0**	*dis.*	*ON*	*OFF*	*ON*	*OFF*	U_h
	0**1**0**0**	*ch.*	*OFF*	*OFF*	*ON*	*OFF*	0
	0**0**0**1**	*ch.*	*OFF*	*OFF*	*OFF*	*OFF*	0

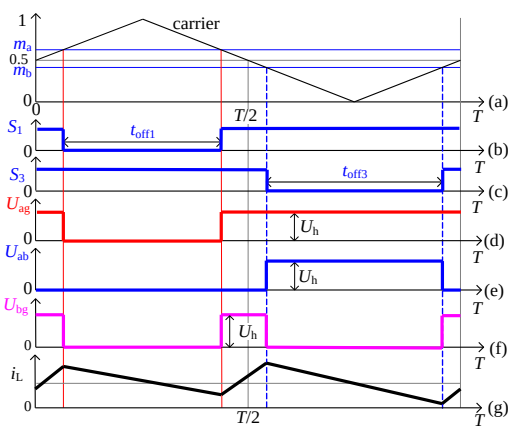

Fig. 2. PWM modulation strategy in the step-down mode (S_2S_4=00).

$$\begin{cases} m_a > U_{carrier}, \ S_1 = 1 \\ m_b < U_{carrier}, \ S_3 = 1 \end{cases} \tag{3}$$

Where m_a and m_b are the modulation indices for the left and right half bridges of the asymmetric H-bridge, $0 < m_b < 0.5 < m_a < 1 < m_a + m_b$ is the limited condition, and $0 \le U_{carrier} \le 1$ is the range of values for the carrier. As a result, the duty cycles of Q_1 and Q_3 move towards 0.5 when m_a and m_b tend to 0.5 according to Fig. 2(a)-(c) and (3). In addition, the frequency of the output PWM voltage U_{bg} is twice the actual switching frequency. The narrower the pulse is, the shorter the inductor charging time exists. In this case, the step-down ratio can be very high. It is noted that the frequency of the inductor current is twice the actual switching frequency, and that the inductor current ripple is half that of the Buck/Boost converter. As a result, a smaller inductance can be adopted to reduce cost and to increase the power density. In the continuous current mode (CCM), the energy W_{ch1} charged in the inductor is equal to the energy W_{dis1} discharged from it in each carrier period T. Equation (4) can be described as:

$$(U_h - U_l) \times (T - t_{off1} - t_{off3}) = U_l \times (t_{off1} + t_{off3}) \tag{4}$$

where t_{off1} and t_{off3} are the "*OFF*" time intervals for Q_1 and Q_3 in each carrier period. In terms of (4), the relationship between the low voltage side U_l and the high voltage side U_h can be written as follows in the step-down mode:

$$\begin{cases} M_{buck} = \dfrac{U_l}{U_h} = m_a - m_b \\ 0 < m_b < 0.5 < m_a < 1 < m_a + m_b \end{cases} \tag{5}$$

where M_{buck} is the step-down ratio, and d_1=m_a=$(T - t_{off1})/T$ and d_3=$1 - m_b$=$(T - t_{off3})/T$ are the duty cycles for the master active power switches Q_1 and Q_3, respectively. In addition, the relationship between m_a and m_b in the step-down mode can be refrained as follows, taking into account the fact that all of the duty cycles are close to 0.5.

$$\begin{cases} m_a = 0.5 + 0.51 M_{buck} \\ m_b = 0.5 - 0.49 M_{buck} \end{cases} \tag{6}$$

When the power flow is from U_l to U_h, the PWM modulation strategy in the step-up mode is shown in Fig. 3. The gate signals S_2 and S_4 for the master active power switches Q_2 and Q_4 are defined by (7).

$$\begin{cases} m_a < U_{carrier}, \ S_2 = 1 \\ m_b > U_{carrier}, \ S_4 = 1 \end{cases} \tag{7}$$

where $0 < m_b < 0.5 < m_a < m_a + m_b < 1$. The duty cycles of Q_2 and Q_4 move towards 0.5 when m_a and m_b approach 0.5 according to Fig. 3(a)-(c) and (7). Furthermore, the output PWM voltage U_{bg} with double the switching frequency can be achieved by means of (2) and Fig. 3(d)-(g). It is noted that the narrower the pulses of U_{bg} are, the shorter the inductor discharge time exists. A high step-up ratio can be obtained. In addition, the frequency of the inductor current is twice the actual switching frequency, and the inductor current ripple is also half that of the Buck/Boost converter, as well as that in the step-down mode. In the CCM, the energy W_{ch2} charged in the inductor is equal to the energy W_{dis2} discharged in each carrier period, and equation (8) can be written as:

$$(U_h - U_l) \times (T - t_{on2} - t_{on4}) = U_l \times (t_{on2} + t_{on4}) \tag{8}$$

where t_{on2} and t_{on4} are the "*ON*" time intervals of Q_2 and Q_4. According to (8), the relationship between U_l and U_h can be obtained as follows in the step-up mode:

$$\begin{cases} M_{boost} = \dfrac{U_h}{U_l} = \dfrac{1}{m_a - m_b} \\ 0 < m_b < 0.5 < m_a < m_a + m_b < 1 \end{cases} \tag{9}$$

where M_{boost} is the step-up ratio, and d_2=$1 - m_a$=t_{on2}/T and d_4=m_b=t_{on3}/T are the duty cycles for Q_2 and Q_4, respectively. Furthermore, the relationship between m_a and m_b in the step-up

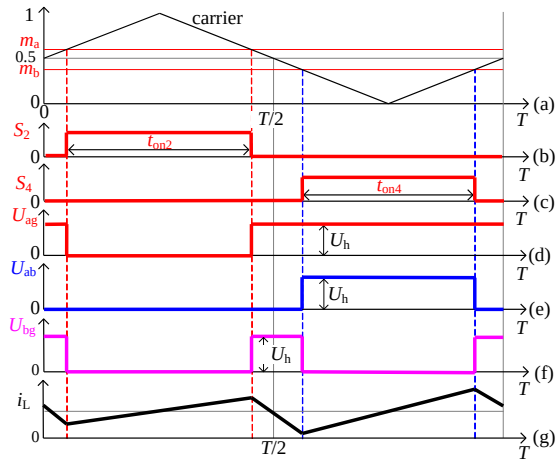

Fig. 3. PWM modulation strategy in step-up mode (S_1S_3=00).

mode can be obtained as follows, considering that all of the duty cycles are as close to 0.5 as possible.

$$\begin{cases} m_a = 0.5 + \dfrac{0.49}{M_{boost}} \\ m_b = 0.5 - \dfrac{0.51}{M_{boost}} \end{cases} \tag{10}$$

Combining (5) and (9), the relationship between U_l and U_h in both directions can be unified as follows:

$$\begin{cases} U_l = U_h \times (m_a - m_b), \\ \text{step-down: } m_a + m_b > 1, \text{ and } \begin{cases} m_a = 0.5 + 0.51M_{buck} \\ m_b = 0.5 - 0.49M_{buck} \end{cases} \\ \text{step-up: } m_a + m_b < 1, \text{ and } \begin{cases} m_a = 0.5 + 0.49 / M_{boost} \\ m_b = 0.5 - 0.51 / M_{boost} \end{cases} \end{cases} \tag{11}$$

where $0 < m_b < 0.5 < m_a < 1$. According to Fig. 2, and Fig. 3, the equivalent carrier frequency of the output PWM voltage is double the actual switching frequency. The wide voltage-gain range of the proposed bidirectional converter always exists without the need for extreme duty cycles as shown in Fig. 4, by means of (6) and (10).

According to Fig. 4, the conventional Buck/Boost converter has a narrower voltage conversion range and suffers from an extreme duty cycle (i.e. over 0.8~0.9) when it operates at a high voltage gain. As for the proposed converter, in the step-down mode, high step-down ratios (e.g. 0.1~0.3) change linearly with the duty cycle. As a result, the required duty cycles d_1 and d_3 are around 0.5 (approximately in the range of 0.55~0.65), as shown in Fig. 4(a). In the step-up mode, although the high step-down ratios (e.g. 3~20) vary in a non-linear manner with the duty cycles d_2 and d_4, the required duty cycles are also around 0.5 (approximately in the range of 0.3~0.475), as shown in Fig. 4(b). Based on the analysis above, the proposed converter has a wider voltage gain range. The duty cycles for all of the semiconductors are kept close to 0.5.

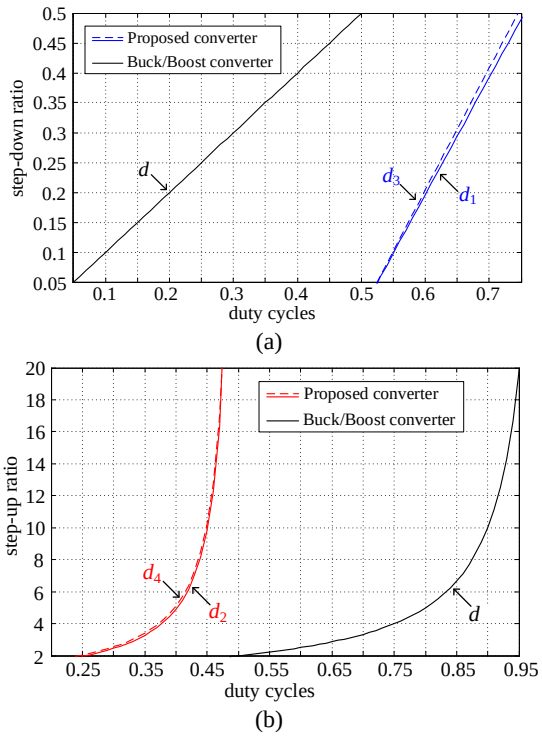

Fig. 4. Comparison of voltage-conversion ranges for the proposed converter and the Buck/Boost converter. (a) In the step-down mode. (b) In the step-up mode.

Even if it operates with a large conversion ratio (i.e. U_h/U_l =20), more appropriate duty cycles (0.475, 0.525) appear, rather than the extremely low duty cycles (i.e. d=0.05 in the step-down mode, and d=0.95 in the step-up mode) in the Buck/Boost converter. It is beneficial to reduce the losses and improve the conversion efficiency.

C. Synchronous Rectification of Slave Active Power Switches

According to Fig. 2 and Fig. 3, master active power switches change according to the power flow direction. There are three switching states for each power flow direction when the slave active power switches operate as a diode rectifier (DR).

$$\begin{cases} [S_1S_2S_3S_4]_{\text{step-down-DR}} = [\mathbf{10}10,\ \mathbf{10}00,\ \mathbf{00}10] \\ [S_1S_2S_3S_4]_{\text{step-up-DR}} = [\mathbf{00}00,\ 0\mathbf{10}0,\ 0\mathbf{00}1] \end{cases} \tag{12}$$

In addition, all four of the active power switches (MOSFETs) of the common grounded asymmetric H-bridge are controlled in a complementary manner as:

$$\begin{cases} S_1 = \overline{S_2} \\ S_3 = \overline{S_4} \end{cases} \tag{13}$$

Therefore, the three DR switching states in each power flow direction can be described by (14), namely the slave active power switches operate as synchronous rectifiers (SR) in each power flow direction. As a result, the slave active power switches can use zero-voltage-switching (ZVS) turn-on and

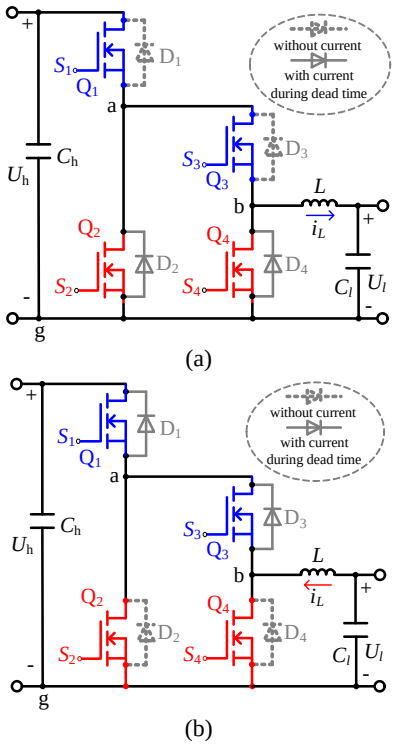

Fig. 5. Synchronous rectification operation principle of the proposed bidirectional converter. (a) Current-flow path in the step-down mode. (b) Current-flow path in the step-up mode.

turn-off, in terms of the dead time t_d for Q_1 and Q_2 in the left half bridge, and Q_3 and Q_4 in the right half bridge.

$$\begin{cases}[S_1S_2S_3S_4]_{\text{step-down-SR}}=[\mathbf{10}10,\ \mathbf{10}01,\ \mathbf{01}10]\\ [S_1S_2S_3S_4]_{\text{step-up-SR}}=[\mathbf{10}10,\ 0\mathbf{11}0,\ 1\mathbf{00}1]\end{cases} \tag{14}$$

The synchronous rectification operation principle of the proposed bidirectional converter is shown in Fig. 5. When it operates in the step-down mode, Q_1 and Q_3 are master active power switches, and Q_2 and Q_4 are slave active power switches, as shown in Fig. 5(a). The anti-parallel diodes D_2 and D_4 follow currents during the dead time t_d for Q_2 and Q_4, leading to zero voltages across Q_2 and Q_4. As a result, Q_2 and Q_4 can obtain the ZVS turn-on and turn-off with the "step-down-SR" switching states in (14).

Similarly, Q_1 and Q_3 change to be slave active power switches, and Q_2 and Q_4 become master active power switches when the converter operates in the step-up mode, as shown in Fig. 5(b). The anti-parallel diodes D_1 and D_3 also follow currents during the dead time t_d for Q_1 and Q_3, resulting in zero voltages across Q_1 and Q_3. Therefore Q_1 and Q_3 can also achieve the ZVS turn-on and turn-off with the "step-up-SR" switching states in (14).

D. Parameters Design of the Capacitor and Inductor

According to Fig. 1(c), Fig. 2 and the operation principle of the bidirectional DC-DC converter in the step-down mode, when S_1S_3=11, Q_1 and Q_3 are turned on, Q_2 and Q_4 are turned off, and the inductor is charging. The charging time in each carrier period is $(d_1+d_3\text{-}1)\times T$, and the high frequency component current of the inductor current flows through the low voltage side capacitor. Then, (15) can be obtained as:

$$\begin{cases}\Delta U_l\times C_l=\dfrac{T}{4}\times\dfrac{\Delta I_{\text{L-Buck}}}{2}\times\dfrac{1}{2}\\ L_{\text{Buck}}\dfrac{\Delta I_{\text{L-Buck}}}{(d_1+d_3-1)T/2}=U_{\text{h}}-U_l\end{cases} \tag{15}$$

where ΔU_l is the voltage ripple of the low voltage side capacitor, and $\Delta I_{\text{L-Buck}}$ is the inductor current ripple in the step-down mode. In addition, $U_l=(d_1+d_3\text{-}1)\times U_{\text{h}}$. Then, the capacitance of the low voltage side capacitor and the inductance L_{Buck} in the step-down mode can be obtained as:

$$\begin{cases}C_l=\dfrac{\Delta I_{\text{L-Buck}}\times T}{16\Delta U_l}\\ L_{\text{Buck}}=\dfrac{U_l(2-d_1-d_3)T}{2\Delta I_{\text{L-Buck}}}\end{cases} \tag{16}$$

Similarly, in the step-up mode, the inductor discharges when S_2S_4=00. The discharging time in each carrier period is $(1\text{-}d_2\text{-}d_4)\times T$. Then, (17) can be achieved as:

$$\begin{cases}C_{\text{h}}\dfrac{\Delta U_{\text{h}}}{(1-d_2-d_4)T/2}=I_{\text{L-Boost}}-I_{\text{o}}\\ L_{\text{Boost}}\dfrac{\Delta I_{\text{L-Boost}}}{(1-d_2-d_4)T/2}=U_{\text{h}}-U_l\end{cases} \tag{17}$$

where ΔU_{h} is the voltage ripple of the high voltage side capacitor, and $\Delta I_{\text{L-Boost}}$ is the inductor current ripple in the step-up mode. In addition, $I_{\text{o}}=(1\text{-}d_2\text{-}d_4)\times I_{\text{L-Boost}}$ is the load current in the high voltage side, $U_l=(1\text{-}d_2\text{-}d_4)\times U_{\text{h}}$. Then, the capacitance of the high voltage side capacitor and the inductance L_{Boost} in the step-up mode can be achieved as:

$$\begin{cases}C_{\text{h}}=\dfrac{I_{\text{o}}(d_2+d_4)T}{2\Delta U_{\text{h}}}\\ L_{\text{Boost}}=\dfrac{U_l(d_2+d_4)T}{2\Delta I_{\text{L-Boost}}}\end{cases} \tag{18}$$

In terms of (16) and (18), the capacitance of the high and low voltage-side capacitors and the inductance of the inductor can be designed as above.

E. Comparisons with Other Bidirectional Solutions

According to the analysis above, comparisons can be drawn among the proposed and other bidirectional solutions in the step-up mode, as shown in Table III. The traditional Buck/Boost converter only needs two semiconductors, and its maximum conversion efficiency is about 94.4%. However, its ideal voltage-gain 1/(1-*d*) is limited due to the effects of parasitic resistance and extreme duty cycles. As a result, it cannot meet the requirements of energy storage system applications. The bidirectional DC-DC converters in [16] and

TABLE III
COMPARISONS OF THE PROPOSED AND OTHER BIDIRECTIONAL SOLUTIONS

Bidirectional Solutions	Voltage Gain	Amount of Semiconductors	Amount of Inductors	Maximum Voltage Stress across Semiconductors	Maximum Current Stress across Semiconductors	Common Ground	Efficiency
Buck/Boost Converter in [30]	$\frac{1}{1-d}U_l$	2	1	U_h	$I_h/(1-d)$	*YES*	83.5% - 94.4%
Converter in [16]	$\frac{1}{(1-d)^2}U_l$	4	2	$U_h+U_h(1-d)$	$\left(\frac{1}{1-d}+\frac{d}{(1-d)^2}\right)I_h$	*YES*	95% - 97.1%
Converter in [26]	$\frac{1+d}{1-d}U_l$	3	2	$\frac{1}{1+d}U_h$	$\frac{1+d}{1-d}I_h$	*NO*	86% - 98%
Converter in [29]	$\frac{1}{1-(d_2+d_3)}U_l$	4	1	U_h	$\frac{1}{1-(d_2+d_3)}I_h$	*NO*	71% - 93.6%
Proposed Converter	$\frac{1}{1-(d_2+d_4)}U_l$	4	1	U_h	$\frac{1}{1-(d_2+d_4)}I_h$	*YES*	83% - 93.5%

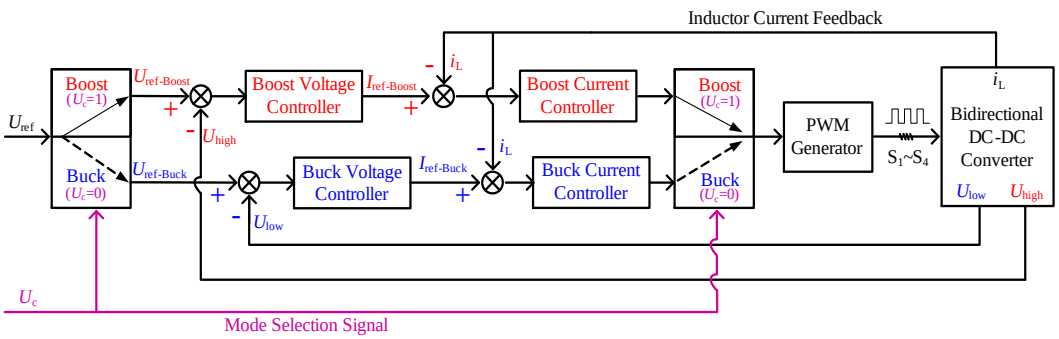

Fig. 6. Control strategy of bidirectional power flows.

[26] achieved a higher voltage-gain. However, these converters need two inductors. In addition, the maximum voltage stress across the semiconductors of the converter in [16] is U_h+U_h(1-d), which increases the switching losses and reduces the conversion efficiency. The potential difference between the output and the input side grounds of the converters in [26] and [29] exists the high frequency PWM voltage (i.e. without a common ground), which may result in more EMI issues. In terms of the proposed asymmetric H-bridge bidirectional DC-DC converter, the number of main components is equal to those of the converters in [16] and [29], and its voltage gain is higher than those in [16] and [26]. In Table III, it is shown that the efficiency of the proposed converter is almost the same as that of the Buck/Boost converter in [30], and that the lowest efficiency increases from 71% with the converter in [29] to 83%, which is a great improvement. The voltage/current stresses on the semiconductors of the proposed converter are the same as those of the Buck/Boost converter under the same input and output voltage/power. In addition, the low and high voltage sides have a common ground, and a high step-up/step-down ratio can be achieved when all of the active power switches operate with duty cycles close to 0.5, which improves the converter's performance and reliability. When compared to the Buck/Boost converter, although two additional semiconductors are required, the proposed converter can achieve a higher voltage gain and a wider voltage conversion range with proper duty cycles. In addition, an effective modulation method reduces the inductor current ripple to half that of the Buck/Boost converter. As a result, a smaller inductance can be adopted to reduce the volume and enhance the dynamic response.

F. Control Strategy of Bidirectional Power Flows

Based on the operation principles in Section III (A~C), a bidirectional power flow control strategy can be achieved as shown in Fig. 6. The feedback voltages U_h and U_l, and the feedback current i_L are sampled by sensors. According to the mode selection signal U_c, the operation modes of the bidirectional DC-DC converter switch between the step-up and the step-down modes. It operates in the step-up mode when U_c=1, and the inductor current i_L is controlled by the Boost current controller with the reference current $I_{ref\text{-}Boost}$ in the current-loop. Meantime, the voltage U_h is controlled by the Boost voltage controller with a reference voltage $U_{ref\text{-}Boost}$ in the voltage-loop. The corresponding PWM scheme, as shown in Fig. 3 and Fig. 5(b), is selected to generate the gate signals S_1~S_4 in the step-up mode. If U_c is changed from "1" to "0", the inductor current i_L is controlled by the Buck current controller

with an opposite direction reference current $I_{ref\text{-}Buck}$, and the voltage U_l is controlled by the Buck voltage controller with a reference voltage $U_{ref\text{-}Buck}$. The corresponding PWM scheme, as shown in Fig. 2 and Fig. 5(a), is selected to generate the gate signals S_1~S_4 in the step-down mode. As a result, the inductor current rises reversely after falling to zero.

IV. Experiment Results and Analysis

In order to validate the feasibility and effectiveness of the proposed converter, a 300W prototype was developed, as shown in Fig. 7. The low voltage side is variable (U_l =24~48V), and the high voltage side is constant (U_h=200V). The bidirectional voltage and current loops are controlled by a TMS320F28335 DSP, and MOSFETs (IXYS-IXFK64N50P) are selected as the active power switches. The switching frequency is f_s=10kHz, the dead time is t_d=1 μs , and the initial value of the inductor is L=306 μH . The experimental parameters are shown in Table IV.

The voltage stress and the gate signals of the slave active power switches in the SR mode of operation are shown in Fig. 8. In the step-down mode, the slave active power switches Q_2 and Q_4 achieve ZVS turn-on and turn-off. The gate signal S_2 and the voltage stress U_{Q2} for Q_2 are shown in Fig. 8(a). In the step-up mode, the slave active power switches Q_1 and Q_3 obtain ZVS turn-on and turn-off. The gate signal S_3 and the voltage stress U_{Q3} for Q_3 are shown in Fig. 8(b). Therefore, the slave active power switches of the proposed bidirectional converter can use ZVS turn-on and turn-off without any extra hardware. This is beneficial to improve conversion efficiency.

The voltages on the high voltage side (constant U_h=200V) and on the continuous variable low voltage side (U_l is between 24V and 48V) are shown in Fig. 9. In the step-down mode, the input voltage is constant at 200V, and the output voltage changes from 24V to 48V continuously over 8 seconds due to the action of the voltage control loop, as shown in Fig. 9(a). The proposed converter can operate over a wide step-down voltage-conversion range (from 0.12 to 0.24). When it operates in the step-up mode, the input voltage changes from 48V to 24V continuously over 8 seconds, and the output voltage remains at a constant 200V due to the action of the voltage control loop, as shown In Fig. 9(b). Therefore, the proposed converter can also operate in a wide step-up voltage-conversion range (from 4.2 to 8.4).

When the proposed converter operates in the step-down mode (converting 200V to 24V), a narrow pulse output PWM voltage U_{bg}=U_{ag} - U_{ab} is needed. The output PWM voltages, the inductor current i_L and the corresponding gate signal- voltage stress are shown in Fig. 10. The PWM voltages U_{ag} and U_{ab} from the half bridges are shown in Fig. 10(a). Then, the narrow pulse output PWM voltage U_{bg} is obtained from U_{ag} - U_{ab} as shown in Fig. 10(b). Therefore, in each switching period T_s=100 μs , the narrow pulse output PWM voltage U_{bg} is double

TABLE IV
Experimental Parameters

Parameters	Values
Rated power P	300W
Storage/filter capacitor C_l	200uF
Storage/filter capacitor C_h	330uF
Storage/filter inductor L	306uH
High voltage side U_h	200V
Low voltage side U_l	24~48V
Switching frequency f_s	10kHz
Power semiconductors Q_1~Q_4	IXYS-IXFK64N50P

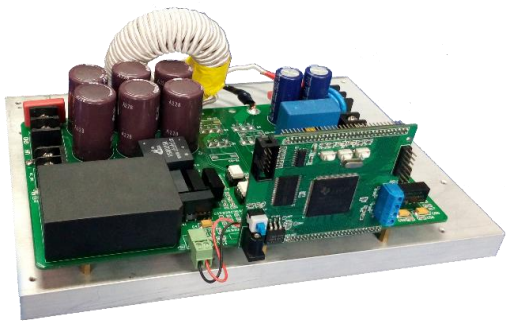

Fig. 7. Experimental prototype of the asymmetric H-bridge bidirectional DC-DC converter.

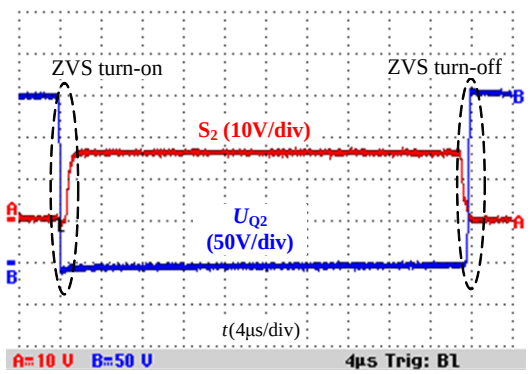

(a)

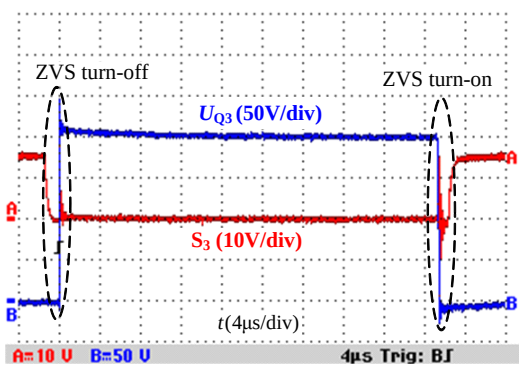

(b)

Fig. 8. Voltage stress and gate signals of the slave active power switches in SR operation. (a) Gate signal and voltage stress of Q_2 in the step-down mode. (b) Gate signal and voltage stress of Q_3 in the step-up mode.

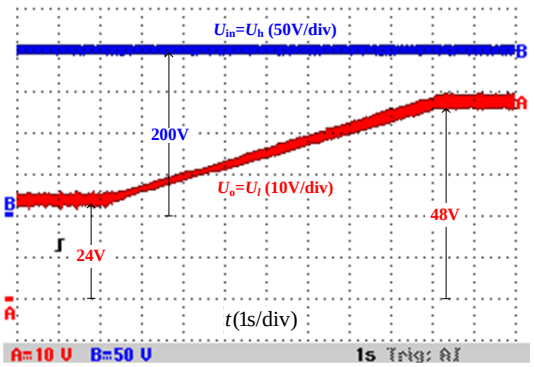

(a) In the step-down mode.

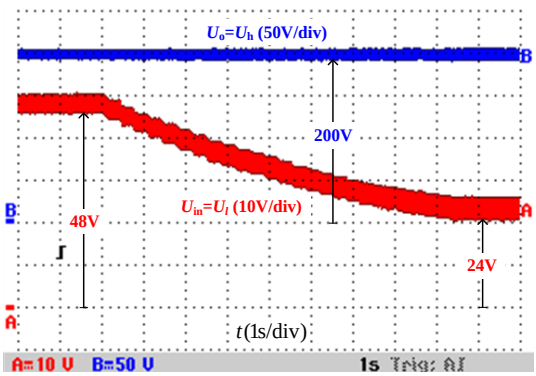

(b) In the step-up mode.

Fig. 9. Voltages on the high voltage side (constant 200V) and the continuous variable low voltage side (between 24V and 48V). (a) In the step-down mode. (b) In the step-up mode.

the actual switching frequency. The inductor is charged when U_{bg} is at 200V (the narrow pulse), and discharged when U_{bg} is at zero, as shown in Fig. 10(b). Although a high step-down ratio is achieved, all of the active power switches operate with proper duty cycles, where d_1≈0.58 is close to 0.5, taking the active power switch Q_1 as an example as shown in Fig. 10(c). It is noted that the inductor of the proposed converter is charged and discharged twice during each switching period. When compared with the Buck/Boost converter, there are two additional power semiconductors in the proposed converter. However, the equivalent switching frequency of the proposed converter is double that of the Buck/Boost converter. The volumes of all the capacitors and inductors in the proposed converter can be reduced by almost half when compared with those of the Buck/Boost converter.

When running in the step-up mode (converting 24V to 200V), a narrow pulse output PWM voltage is also needed. The output PWM voltages, the inductor current i_L and the corresponding gate signal-voltage stress are shown in Fig. 11. The PWM voltages U_{ag} and U_{ab} from the half bridges are shown in Fig. 11(a), and the narrow pulse output PWM voltage U_{bg} is obtained from U_{ag} - U_{ab} as shown in Fig. 11(b). Therefore, in each switching period T_s=100 μs , the narrow pulse output PWM voltage U_{bg} is double the actual switching frequency. The inductor is charged when U_{bg} is at zero, and it is

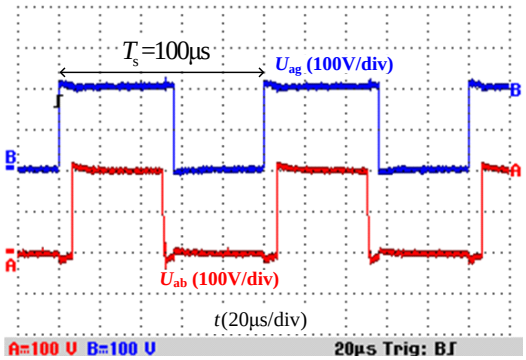

(a)

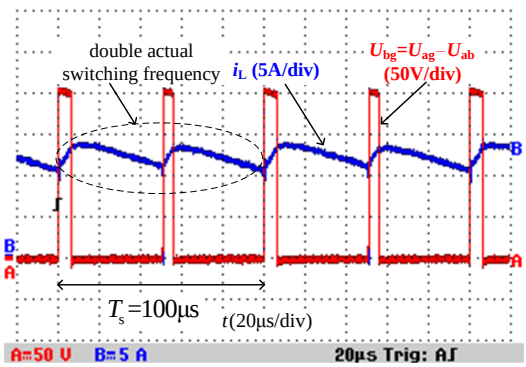

(b)

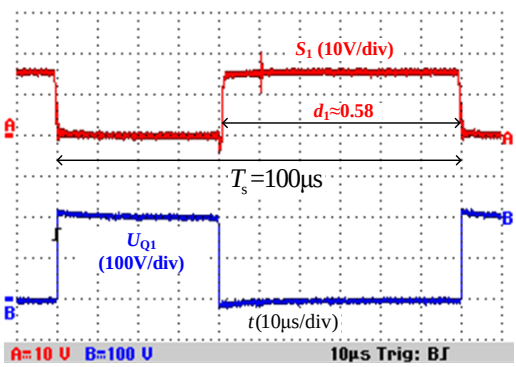

(c)

Fig. 10. Output PWM voltages, inductor current i_L and the corresponding gate signal-voltage stress in the step-down mode. (a) U_{ag} and U_{ab}. (b) U_{bg} and the inductor current i_L. (c) S_1 and U_{Q1}.

discharged when U_{bg} is at 200V (the narrow pulse), as shown in Fig. 11(b). Although a high step-down ratio is obtained, all of the active power switches operate with the proper duty cycles, where d_4≈0.44 is close to 0.5, taking the active power switch Q_4 as an example as shown in Fig. 11(c). In addition, similar to the step-down mode, the inductor of the proposed converter is also charged and discharged twice during each switching period.

Experimental results of the bidirectional operation of the proposed converter between the step-down and the step-up modes are shown in Fig. 12. The high voltage side is connected to a DC-link bus (at a constant 200V), and the low voltage side is connected to battery stacks (nominal 48V). In order to easily

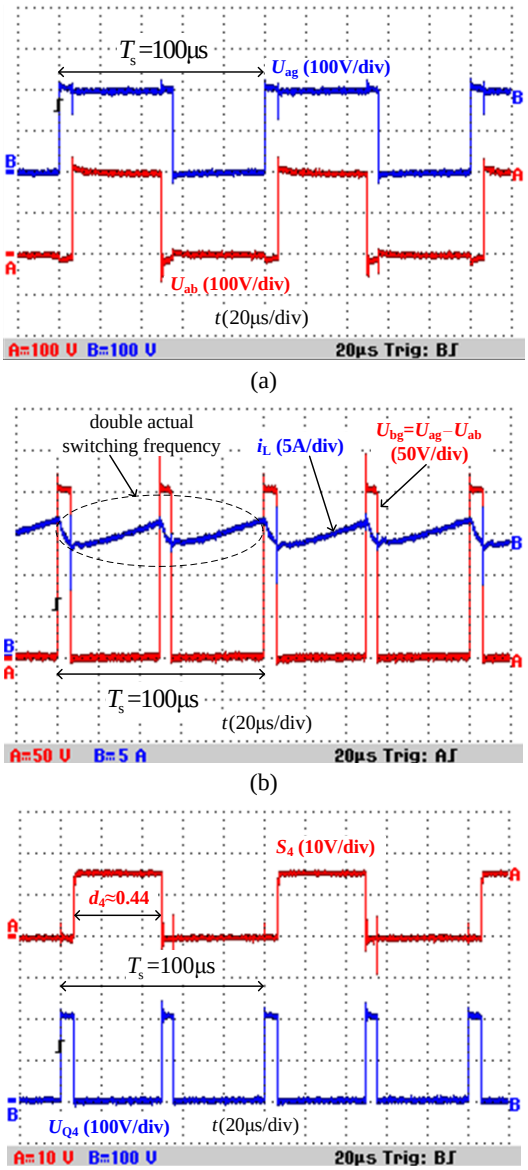

Fig. 11. Output PWM voltages, inductor current i_L and the corresponding gate signal-voltage stress in the step-up mode. (a) U_{ag} and U_{ab}. (b) U_{bg} and the inductor current i_L. (c) S_4 and U_{Q4}.

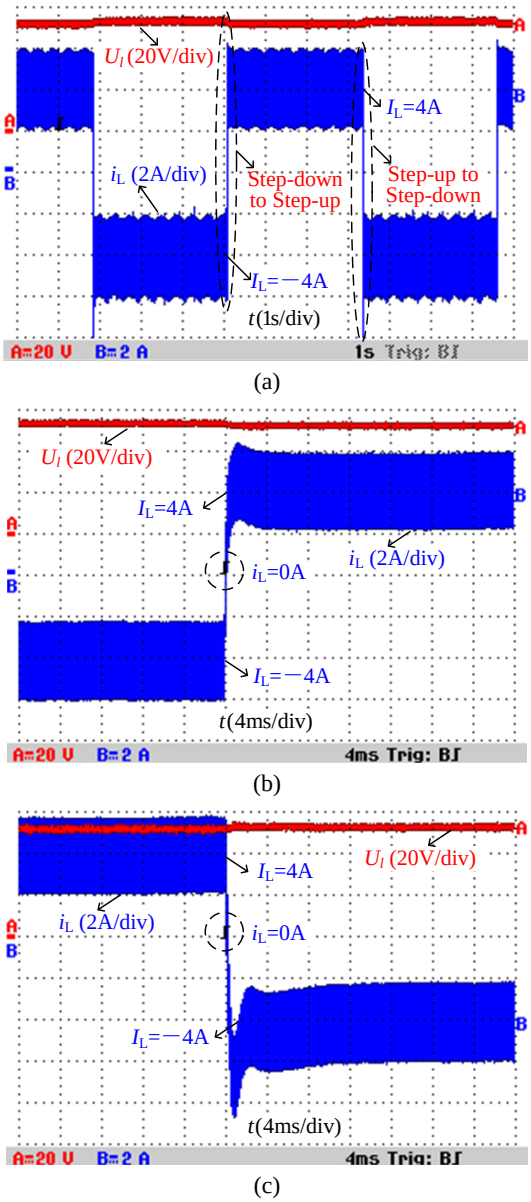

Fig. 12. Experimental results of bidirectional operation between the step-down and the step-up modes. (a) Processes of step-up to step-down and step-down to step-up. (b) Transient process of the step-down to step-up mode (I_L=−4A to 4A). (c) Transient process of the step-up to step-down mode (I_L=4A to -4A).

control the power flow between the battery stacks and the DC-link bus, the proposed converter, which is controlled as a current source converter, acts as an interface between them. In Fig. 12(a), the converter steps down with the reference inductor current I_L= - 4A, and the power flow is from the DC-link bus to the batter stacks (U_l=54V). When the converter is controlled to operate continuously from the step-down mode to the step-up mode, the converter works in the step-up mode with the reference inductor current I_L=4A, and the power flow is from the battery stacks (U_l=52V) to the DC-link bus. The detailed transient process of the step-down to the step-up mode (I_L= - 4A to 4A) is shown in Fig. 12(b). The current of the battery stacks changes from - 4A to 4A over 3.2ms. In other words, the battery stacks are charged with a constant current of 4A before the controlled power flow command comes. Then, the battery current falls to zero (i_L=0) quickly, and the battery stacks switch to be discharged with a constant current of 4A over 3ms. The detailed transient process of the step-up to the step-down mode (I_L=4A to - 4A) is shown in Fig. 12(c). The battery current falls rapidly to zero (i_L=0) to switch the operating mode after the new power flow command comes. Then, the charged current of the battery stacks stabilizes at a constant current of 4A over 8ms. From Fig. 12, it can be seen that the proposed converter can respond quickly to the control signal under the current control loop. This is due to the effective modulation method and the reduced inductance.

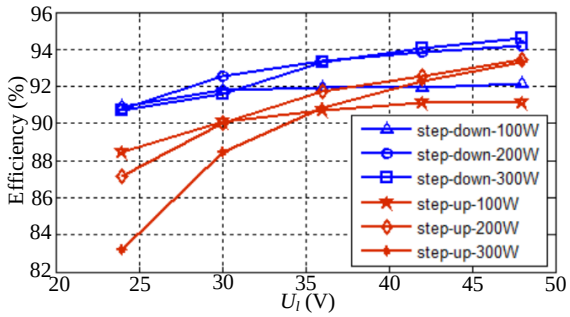

Fig. 13. Conversion efficiency of the proposed bidirectional converter at different voltages of low voltage side and load powers (U_l=24~48V, U_h=200V).

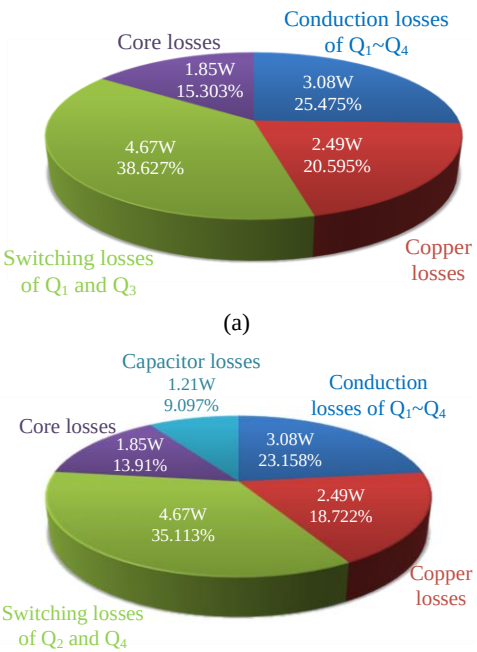

Fig. 14. Calculated power loss distributions for the experiment when U_l=48V, U_h=200V, P=300W. (a) In the step-down mode. (b) In the step-up mode.

The conversion efficiency of the proposed bidirectional converter at different voltages on the low voltage side (24V to 48V) and at different load powers (100W to 300W) has been measured using a Yokogawa-WT3000 Power Analyzer, as shown in Fig. 13. In the step-down mode, the input voltage is 200V. The minimum efficiency is 90.7% when the output voltage is 24V and the load power is 300W, while the maximum efficiency is 94.7% when the output voltage is 48V and the load power is 300W. In the step-up mode, the output voltage is set as 200V. The minimum efficiency is 83% when the input voltage is 24V and the load power is 300W, while the maximum efficiency is 93.5% when the input voltage is 48V and the load power is 200W. Therefore, the conversion efficiency improves by increasing voltage on the low voltage side.

The calculated power loss distributions for the experiment when U_l=48V, U_h=200V and P=300W are shown in Fig. 14. In the step-down mode, the total losses of the converter are 12.09W, and the loss distribution is shown in Fig. 14(a). By analyzing the power losses distribution, it can be concluded that the major losses come from the power switches Q_1 and Q_3. The turn-on, turn-off and conduction losses of Q_1 and Q_3 account for 38.627% of the total losses. The conduction losses of the power switches Q_1~Q_4 account for 25.475% of the total losses. The conduction losses and the core loss of the inductor account for 20.595% and 15.303% of the total losses, respectively. In the step-up mode, the total losses of the converter are 13.3W, and Fig. 14(b) shows the loss distribution. The largest power losses are the turn-on and turn-off losses of Q_2 and Q_4 and the conduction losses of Q_1~Q_4, which account for 58.271% of the total losses. The losses of the capacitors and the copper loss of the inductor account for 27.819% of the losses, and the remaining 13.91% of the total losses is the core loss of the inductor.

V. Conclusions

A wide-voltage-conversion range bidirectional DC-DC converter is proposed in this paper. A high step-down/step-up ratio can be achieved by using one typical *LC* energy storage component and a special common grounded asymmetric H-bridge comprised of four active power switches with anti-parallel diodes, instead of a transformer, a switched-capacitor, and a coupled-inductor or a Z-source net. In addition, its slave active power switches can achieve ZVS turn-on and turn-off without any extra hardware, and the equivalent frequency of the output PWM voltage is twice as high as the actual switching frequency. A 300W prototype obtains a maximum conversion efficiency of 94.7% in the step-down mode and 93.5% in the step-up mode. Therefore, the proposed bidirectional topology with a common ground is suitable for the energy storage systems of renewable applications and hybrid energy source electric vehicle applications.

Acknowledgment

This work was supported in part by the National Natural Science Foundation of China under Grant 51577130, and in part by the Research Program of Application Foundation and Advanced Technology of Tianjin, China under Grant 15JCQNJC03900.

References

[1] B. Singh and R. Kumar, "Solar photovoltaic array fed water pump driven by brushless DC motor using Landsman converter," *IET Renew. Power Gener.*, Vol. 10, No. 4, pp. 474-484, Apr. 2016.

[2] M. S. Mahmoud, M. S. U. Rahman, and F. M. A.L.-Sunni, "Review of microgrid architectures–a system of systems perspective," *IET Renew. Power Gener.*, Vol. 9, No. 8, pp.

1064-1078, Nov. 2015.

[3] J. d. Santiago, H. Bernhoff, B. Ekergard, S. Eriksson, S. Ferhatovic, R. Waters, and M. Leijon, "Electrical motor drivelines in commercial all-electric vehicles: A review," *IEEE Trans. Veh. Technol.*, Vol. 61, No. 2, pp. 475-484, Feb. 2012.

[4] C. C. Chan, "The state of the art of electric and hybrid vehicles," *Proceedings of the IEEE*, Vol. 90, No. 2, pp. 247-275, Feb. 2002.

[5] D. Wu, F. Tang, T. Dragicevic, J. C. Vasquez, and J. M. Guerrero, "A control architecture to coordinate renewable energy sources and energy storage systems in islanded microgrids," *IEEE Trans. Smart Grid*, Vol. 6, No. 3, pp. 1156-1166, May 2015.

[6] N. L. Diaz, T. Dragicevic, J. C. Vasquez, and J. M. Guerrero, "Intelligent distributed generation and storage units for DC microgrids – A new concept on cooperative control without communications beyond droop control," *IEEE Trans. Smart Grid*, Vol. 5, No. 5, pp. 2476-2485, Sep. 2014.

[7] H. Yoo, S. Sul, Y. Park, and J. Jeong, "System integration and power-flow management for a series hybrid electric vehicle using supercapacitors and batteries," *IEEE Trans. Ind. Appl.*, Vol. 44, No. 1, pp. 108-114, Jan./Feb. 2008.

[8] K. Hu, P. Yi, and C. Liaw, "An EV SRM drive powered by battery/supercapacitor with G2V and V2H/V2G capabilities," *IEEE Trans. Ind. Electron.*, Vol. 62, No. 8, pp. 4714-4727, Aug. 2015.

[9] K. Wu, C. W. d. Silva, and W. G. Dunford, "Stability analysis of isolated bidirectional dual active full-bridge DC–DC converter with triple phase-shift control," *IEEE Trans. Power Electron.*, Vol. 27, No. 4, pp. 2007-2017, Apr. 2012.

[10] N. Denniston, A. M. Massoud, S. Ahmed, and P. N. Enjeti, "Multiple-module high-gain high-voltage DC–DC transformers for offshore wind energy systems," *IEEE Trans. Ind. Electron.*, Vol. 58, No. 5, pp.1877-1886, May 2011.

[11] A. Rodriguez, A. Vazquez, D. G. Lamar, M. M. Hernando, and J. Sebastian, "Different purpose design strategies and techniques to improve the performance of a dual active bridge with phase-shift control," *IEEE Trans. Power Electron.*, Vol. 30, No. 2, pp. 790-804, Feb. 2015.

[12] A. Ajami, H. Ardi, and A. Farakhor, "A novel high step-up DC/DC converter based on integrating coupled inductor and switched-capacitor techniques for renewable energy applications," *IEEE Trans. Power Electron.*, Vol. 30, No. 8, pp. 4255-4263, Aug. 2015.

[13] R. J. Wai and R. Y. Duan, "High-efficiency bidirectional converter for power sources with great voltage diversity," *IEEE Trans. Power Electron.*, Vol. 22, No. 5, pp. 1986-1996, Sep. 2007.

[14] H. Wu, K. Sun, L. Zhu, L. Chen, and Y. Xing, "High step-up/step-down soft-switching bidirectional DC-DC converter with coupled-inductor and voltage matching control for energy storage systems," *IEEE Trans. Ind. Electron*, Vol. 63, No. 5, pp. 2892-2903, May 2016.

[15] C.-C. Lin, L.-S. Yang, and G. W. Wu, "Study of a non-isolated bidirectional DC-DC converter," *IET Power Electron.*, Vol. 6, No. 1, pp. 30-37, Jan. 2013.

[16] H. Ardi, A. Ajami, F. Kardan, and S. N. Avilagh, "Analysis and implementation of a nonisolated bidirectional DC-DC converter with high voltage gain," *IEEE Trans. Ind. Electron.*, Vol. 63, No. 8, pp. 4878-4888, Aug. 2016.

[17] M. Kwon, S. Oh, and S. Choi, "High gain soft-switching bidirectional dc-dc converter for eco-friendly vehicles," *IEEE Trans. Power Electron.*, Vol. 29, No. 4, pp. 1659-1666, Apr. 2014.

[18] P. Jose and N. Mohan, "A novel ZVS bidirectional cuk converter for dual voltage systems in automobiles," in *Proc. IEEE IECON Conf. Rec.*, pp. 117-122, 2003.

[19] I.-D. Kim, S.-H. Paeng, J.-W. Ahn, E.-C. Nho, and J.-S. Ko, "New bidirectional ZVS PWM Sepic/Zeta DC–DC converter," in *Proc. IEEE ISIE Conf. Rec.*, pp. 555-560, 2007.

[20] R. J. Wai and R. Y. Duan, "High-efficiency bidirectional converter for power sources with great voltage diversity," *IEEE Trans. Power Electron.*, Vol. 22, No. 5, pp. 1986-1996, Sep. 2007.

[21] P. U R, and A. K. Rathore, "Extended range ZVS active-clamped current-fed full-bridge isolated DC/DC converter for fuel cell applications: analysis, design, and experimental results," *IEEE Trans. Ind. Electron.*, Vol. 60, No. 7, pp.2661-2672, Jul. 2013.

[22] L. Jiang, C. C. Mi, S. Li, M. Zhang, X. Zhang, and C. Yin, "A novel soft-switching bidirectional DC–DC converter with coupled inductors," *IEEE Trans. Ind. Appl.*, Vol. 49, No. 6, pp. 2730-2740, Nov./Dec. 2013.

[23] Y.-F. Wang, L.-K. Xue, C.-S. Wang, P. Wang, and W. Li, "Interleaved high-conversion-ratio bidirectional DC-DC converter for distributed energy-storage systems – Circuit generation, analysis, and design," *IEEE Trans. Power Electron.*, Vol. 31, No. 8, pp. 5547-5561, Aug. 2016.

[24] S.-C. Tan, S. Kiratipongvoot, S. Bronstein, A. Ioinovici, Y. M. Lai, and C. K. Tse, "Adaptive mixed on-time and switching frequency control of a system of interleaved switched-capacitor converters," *IEEE Trans. Power Electron.*, Vol. 26, No. 2, pp. 364-380, Feb. 2011.

[25] B. Wu, K. Smedley, and S. Sigmond, "A new 3X interleaved bidirectional switched capacitor converter," in *Proc. IEEE Appl. Power Electron. Conf. Expo.*, pp. 1433-1439, 2014.

[26] O. Cornea, G. Andreescu, N. Muntean and D. Hulea, "Bidirectional power flow control in a dc microgrid through a switched-capacitor cell hybrid DC-DC converter," *IEEE Trans. Ind. Electron.*, Vol. 64, No. 4, pp. 3012-3022, Apr. 2017.

[27] J. Zhang and J. Ge, "Analysis of Z-source DC-DC converter in discontinuous current mode," in *Proc. Power Energy Eng. Conf.* (*APPEEC*), pp. 1-4, 2010.

[28] H. Shen, B. Zhang, D. Qiu, and L. Zhou, "A common grounded Z-source DC-DC converter with high voltage gain," *IEEE Trans. Ind. Electron.*, Vol. 63, No. 5, pp.2925-2935, May 2016.

[29] Y. Zhang, Y. Gao, J. Li, M. Sumner, P. Wang, and L. Zhou, "High ratio bidirectional DC-DC converter with synchronous rectification H-bridge for hybrid energy sources electric vehicles," *J. Power Electron.*, Vol. 16, No. 6, pp. 2035-2044, Nov. 2016.

[30] B. Wang, J. Xu, R. J. Wai, and B. Cao, "Adaptive sliding-mode with hysteresis control strategy for simple multimode hybrid energy storage system in electric vehicles," *IEEE Trans. Ind. Electron.*, Vol. 64, No. 2, pp.1404-1414, Feb. 2017.

Yun Zhang (M'13) was born in Jiangsu, China, in 1980. He received his B.S. and M.S. degrees in Electrical Engineering from the Harbin University of Science and Technology, Harbin, China, in 2003 and 2006, respectively; and his Ph.D. degree in Electrical Engineering from the Harbin Institute of Technology, Harbin, China, in 2010. In 2010, he joined Tianjin University, Tianjin, China, as a Lecturer in the School of Electrical and Information Engineering, where he is presently working as an Associate Professor. His current research interests include topologies, modulation, and control strategies for the power converters of electric vehicles and microgrids. Dr. Zhang is an Associate Editor of the Journal of Power Electronics.

Yongping Gao was born in Shanxi, China. He received his B.S. degree in Electrical Engineering from the China University of Mining and Technology, Xuzhou, China, in 2015. He is presently working towards his M.S. degree in Electrical Engineering from Tianjin University, Tianjin, China. His current research interests include power electronics converters and energy management.

Jing Li (M'15) was born in Beijing, China. She received her B.S. (with Honors) and M.S. (with Distinction) degrees from the Beijing Institute of Technology, Beijing, China, in 1999 and 2002, respectively; and her Ph.D. degree from the University of Nottingham, Nottingham, ENG, UK, in 2010. She subsequently worked as a Research Fellow within the Power Electronic, Machine and Control Group (PEMC), University of Nottingham. She is presently working as a Lecturer in the Department of Electrical and Electronic Engineering, University of Nottingham Ningbo China, Ningbo, China. Her current research interests include condition monitoring for motor drive systems and power distribution systems, and the advanced control and design of motor drive systems.

Mark Sumner (SM'05) received his B.S. degree in Electrical and Electronic Engineering from Leeds University, Leeds, ENG, UK, in 1986; and his Ph.D. degree in Induction Motor Drives from the University of Nottingham, Nottingham, ENG, UK, in 1990. After graduating, he worked as a Research Assistant and he became a Lecturer in 1992. He is presently working as a Professor of Electrical Energy Systems. His current research interests include the control of power electronic systems including sensorless motor drives, diagnostics and prognostics for drive systems, power electronics for enhanced power quality and novel power system fault location strategies.